Modification of the SUMO activating enzyme subunit SAE2 directs SUMO isoform bias required for mitotic fidelity.

Alexandra K. Walker[1*], Alexander J. Lanz[1*], Mohammed Jamshad[1], Alexander J. Garvin[1], Peter Wotherspoon[2], Benjamin F. Cooper[2], Timothy J. Knowles[2] and Joanna R. Morris[1,3].

1. Birmingham Centre for Genome Biology and Institute of Cancer and Genomic Sciences, College of Medical and Dental Schools, University of Birmingham, B15 2TT, U.K.

2. School of Biosciences, University of Birmingham, Birmingham, B15 2TT, U.K.

3. Correspondence: j.morris.3@bham.ac.uk

*. Joint First authors.

Keywords: SUMO, SUMO1, SUMO2/3, E1, SAE1, SAE2, HDAC.

Abstract. Protein conjugation with the Small Ubiquitin-like Modifier SUMO1 or the related SUMO2/3 drive changes to protein behaviour. Many substrates are found modified by both SUMO1 and SUMO2/3, while others are modified by one or the other. How isoform specificity is directed is poorly understood. Here we examine modification of the catalytic component of the human SUMO Activation Enzyme, SAE2. We find that an acetylated K164-SAE2 analogue preferentially activates SUMO2 in competition with SUMO1, and that K164-SAE2 discriminates paralogues through their C-terminal regions. We find that K164-SAE2 is deacetylated during mitosis. Mitotic defects in cells expressing an acetylated K164-SAE2 analogue can be corrected by over-expression of SUMO1, suggesting SUMO1 conjugation driven by the deacetylated enzyme supports mitotic fidelity. These surprising data reveal that modification of the SUMO-activating enzyme can bias SUMO paralogue conjugation.

Introduction.

There are several ubiquitin-like small modifiers in mammals, including the Small Ubiquitin-like Modifiers (SUMOs) (Ilic, Magnussen et al., 2022). Higher eukaryotes express SUMO paralogues belonging to two subfamilies, SUMO-1, and the highly similar SUMO-2 and SUMO-3, referred to as SUMO-2/3. SUMOylation contributes to many intracellular processes, including transcription, DNA repair, chromatin remodelling, signal transduction, and mitosis (Chang & Yeh, 2020, Garvin & Morris, 2017). In the initial step of the cascade, SUMO activation is catalysed by the SUMO E1 heterodimer comprised of SUMO-activating enzyme 1 (SAE1/ AOS1) and 2 (SAE2/UBA2)(Desterro, Rodriguez et al., 1999, Johnson, Schwienhorst et al., 1997, Okuma, Honda et al., 1999); referred to as SAE1/SAE2 herein. The E1 recognises SUMO and ATP-Mg^{2+} via its adenylation catalytic site and initiates the conjugation process by adenylating the SUMO C-terminus. Subsequently, a thioester bond forms between SUMO and the active-site cysteine residue, C173 in SAE2 (Lois & Lima, 2005). The activated SUMO is transferred to the catalytic cysteine in the only SUMO E2 conjugating enzyme, UBC9 (Johnson & Blobel, 1997). The SUMO can then be transferred to a target lysine directly from the UBC9 or with the added guidance of a SUMO E3 ligase.

Thousands of proteins are reported to be SUMOylated and deSUMOylated in a spatially and temporally controlled manner (Becker, Barysch et al., 2013, Hendriks, Lyon et al., 2018, Hendriks, Lyon et al., 2017, Hendriks & Vertegaal, 2016). SUMO-1 is conjugated to its substrates chiefly as a single conjugate (mono-SUMOylation), whereas SUMO-2/3 can form chains (poly-SUMOylated) (Ulrich, 2008). SUMO-1 is found in cells conjugated to proteins, whereas SUMO-2/3 can be found in their free forms, and their conjugation to substrates increases following cellular stresses (Ilic et al., 2022). Some substrates are preferentially modified by SUMO1 or SUMO2/3 (Becker et al., 2013). Two broad mechanisms are known to contribute to isoform biases. The first is driven by the differential specificity of SUMO interaction motifs (SIMs) toward SUMO paralogues (Namanja, Li et al., 2012). SIMs within SUMO E3s and target proteins contribute to bias SUMO paralogue-specific modification (Chang, Izumiya et al., 2009, Gareau, Reverter et al.,

2012, Meulmeester, Kunze et al., 2008, Reverter & Lima, 2005, Tatham, Kim et al., 2005, Zhu, Zhu et al., 2008). In the second mechanism, proteins may be modified by all isoforms, but one SUMOylated species is protected from isopeptidases, e.g. RanGAP1 can form an isopeptidase-resistant complex with RanBP2 and Ubc9 only when modified with SUMO1 but not when modified with SUMO2/3 (Werner, Flotho et al., 2012, Zhu, Goeres et al., 2009).

Here we identify a means of paralogue-conjugation bias not previously described. We investigate the modification of the SUMO activating enzyme, SAE1/SAE2. We find that SAE2 is deacetylated during mitosis and after irradiation. A form of SAE2, similar to the acetylated form, K164Q-SAE2, exhibits a reduced ability to activate SUMO1 when SUMO2 is present. K164Q-SAE2 has no detected DNA damage repair defect, but results in defective mitotic features such as multipolar spindles. SUMO1 overexpression reverses spindle defects in K164Q-SAE2 expressing cells. These data show isoform bias can be introduced in the supply of active SUMO isoform available to the conjugation machinery, revealing a new mechanism employed to direct SUMO paralogue conjugation.

Results.

K164-SAE2 is acetylated. Using an acetylated K164-SAE2 peptide, we generated a monoclonal antibody. We tested the antibody on immunoprecipitates of WT-SAE2, and on a form of SAE2 that cannot be acetylated at K164, K164R-SAE2 (Fig. 1a). AcK164-SAE2 could be detected in asynchronous cells and was reduced in asynchronous cells an hour after irradiation exposure (10 Gy). The signal was also reduced in cells synchronised in mitosis by 17-hour treatment with the microtubule polymerisation inhibitor nocodazole (Fig. 1a & b). We tested several inhibitors of deacetylases and noted that the pan-Histone Deactylase (HDAC) inhibitor panobinostat suppressed loss of the signal on nocodazole treatment, as did the selective HDAC6 inhibitor, ACY-738 (Jochems, Boulden et al., 2014) (Fig. 1b & c). These data suggest SAE2 is acetylated at K164 and that some cellular stresses and cell cycle stages lead to its deacetylation.

K164Q-SAE2 has an altered SUMO bias. K164-SAE2 is close to the SUMO binding pocket of the E1 (Hann, Ji et al., 2019, Lois & Lima, 2005). This led us to address if K164-SAE2 acetylation might have an impact on SUMO interactions. We generated heterodimer proteins *in vitro* in which the SAE2 element carried a mutation at codon 164 to glutamine (Q) (Supp. Fig. 1a). Glutamine resembles the uncharged functional group of acetylation, and although not forming classical isosteres, glutamine has been used as an acetyl mimic (e.g. (Bhardwaj & Das, 2016, Kim, Sprung et al., 2006)). We labelled WT SAE1/SAE2 and SAE1/K164Q-SAE2 with NT-647-NHS for MicroScale Thermophoresis (MST). The technique detects the movement of fluorophore-tagged molecules in a temperature gradient. The thermophoresis of a protein differs from that of its liganded complex such that MST can be used to quantify interaction dissociation constants (Wienken, Baaske et al., 2010). We subjected labelled E1 heterodimers to MST analysis with increased concentrations of SUMO1 or SUMO2. Fitting of the data to the change in thermophoresis showed WT-E1 has a greater affinity (lower K_d) for SUMO1 than SUMO2 (Fig. 2a and Supp. Fig. 2a), consistent with K_m measurements of SUMO1 *Vs* SUMO2 with AOS1/UBA2 (Wiryawan, Dan et al., 2015). In contrast, the K164Q-SAE2 E1 had a greater affinity (lower K_d) for the SUMO2 isoform and reduced affinity for SUMO1 (Fig. 2a).

We next monitored the activation capacity of wild-type and E1 mutants by assessing SUMO1 loading onto SAE2 in non-reducing gels, observed as a decrease in SAE2 motility in the presence of ATP and SUMO1. Reactions supplemented with the Ubl-modifier FAT10, able to compete for the SUMO (Aichem, Sailer et al., 2019), reduced the intensity of the slow-moving WT-SAE2 at ~120 kDa, consistent with this band representing SUMO1~SAE2 (Fig. 2b and Supp. Fig. 2b). We compared the ability of E1 bearing K164Q-SAE2 or K164R-SAE2 to activate SUMO1 and noted that SAE2-K164Q showed reduced SUMO1~SAE2. E1 bearing WT-SAE2 and K164R-SAE2 showed similar SUMO1~SAE2 proportions and were competed to a similar degree by FAT10 (Fig. 2b). We next tested SUMO1 *Vs* SUMO2 competition by incubating SAE1/SAE2 with SUMO paralogues in which one was GST-tagged at the N-terminus, adding 27 kDa, enabling loaded SUMO-isoforms to be distinguished. We found that WT-E1 and K164R-SAE2 E1 were able to form GST-SUMO1~SAE2 in the presence of SUMO2, whereas K164Q-SAE2 E1 formed less GST-SUMO1~SAE2 in its presence (Fig. 2c). In agreement, when the GST was fused to SUMO2, the formation of the smaller SUMO1~SAE2 was less evident on K164Q-SAE2 E1 (Fig. 2c). To test whether the reduced activation by K164Q-SAE2 E1 influences SUMOylation of a substrate, we returned to using untagged SUMO1 and SUMO2, and included UBC9 and a model substrate, the RanGAP1 fragment

(amino acids 398-587). All SUMO E1 variants could promote the SUMOylation of RanGAP1 to a comparable degree when supplied with a single SUMO isoform. In contrast, when supplied with equimolar amounts of SUMO1 and SUMO2, K164Q-SAE2 E1 drove increased SUMO2-RanGAP1 modification and reduced SUMO1-RanGAP1 conjugation compared to WT or K164R-SAE2 E1 (Fig. 2d and Supp. Fig. 2c & d). These data show K164Q-SAE2 E1 is less able to promote SUMO1 conjugation in the presence of SUMO2.

To address how K164-SAE2 could discriminate between SUMO paralogues, we examined the structures of SAE1:SAE2-SUMO-AVSN (Hann et al., 2019, Olsen, Capili et al., 2010) and noted potential proximity between SAE2-K164 and E93 of SUMO1 (Fig. 2e). Intriguingly, the equivalent residue in SUMO2 is charge-neutral, Q89. To test the idea that the E1 discriminates between isoforms through these residues, we swapped them, creating E93Q-SUMO1 and Q89E-SUMO2. Remarkably, these mutants were able to switch the bias of K164Q-SAE2 E1, from promoting SUMO2, with poor SUMO1 conjugation, to promoting SUMO1 with poor SUMO2 conjugation (Fig. 2f). These data are consistent with the idea that K164-SAE2 interaction with the SUMO paralogue C-terminal region contributes to isoform conjugation bias.

K164-SAE2 supports mitotic fidelity. To address the potential cellular consequences of K164 modification, we generated a dual expression system for siRNA-resistant SAE1/SAE2 and tested both the unacetylatable K164R-SAE2, the acetyl near-mimic K164Q-SAE2, and mutated the active cysteine, C173G (Desterro et al., 1999). We examined bulk SUMO conjugates in cells depleted and complemented with SAE2 variants. Those with C173G-SAE2 had low conjugate levels, and while those complemented with K164Q-SAE2 E1 had less abundant global SUMO1 conjugates than K164R-SAE2 E1 complemented cells, the difference was subtle(Fig. 3a), suggesting the impact of the K-Q mutation in cells using this system is less pronounced than observed *in vitro.*

We then tested complemented cells for potential defects in phenotypes driven by SUMO modifications. Depletion of SAE1/SAE2 resulted in cellular sensitivity to a temperature of 43 °C that could be suppressed by complementation with WT-SAE2, K164Q-SAE2, or K164R-SAE2 (Fig. 3b), indicating little or no influence of the K164-SAE2 modification on the response to heat-shock. Further, we found no impact of K164-SAE2 mutations on the resolution of the DNA damage marker γH2AX after exposure to irradiation and observed only a moderate impact of SAE1/SAE2 depletion on the repair of enzymatically generated DNA breaks (Supp. Fig. 3b-d). Despite the critical role of SUMO in the cellular response to damaged DNA (Garvin & Morris, 2017), these findings are consistent with the report that inhibition of the SUMO E1 has little impact on the cellular response to DNA damaging agents, cisplatin or hydroxyurea (He, Riceberg et al., 2017).

One of the most SUMO1ylated cellular proteins is RanGAP1 (Becker et al., 2013), where SUMO1 performs a structural role making up the composite RanBP2/RanGAP1-SUMO1/Ubc9 complex (Flotho & Werner, 2012, Reverter & Lima, 2005, Werner et al., 2012). RanGAP1-SUMO1 is concentrated at the kinetochore of mitotic spindles and contributes to stable kinetochore: microtubule association (Joseph, Liu et al., 2004, Joseph, Tan et al., 2002). SUMO1 modification of RanGAP1 is stable over several cell cycles, even in the presence of E1 inhibition (He et al., 2017), so to examine whether E1 modifications might impact RANGAP1-SUMO1, we expressed exogenous SAE1/SAE2 over seven days and performed sequential siRNA depletions before synchronising cells with nocodazole. Under these conditions, cells expressing C173G-SAE2 or K164Q-SAE2 exhibited reduced RanGAP1-SUMO1 compared to cells expressing WT-SAE2 or K164R-SAE2 (Fig. 3c & d). These data suggest that modification of K164 can influence SUMO1-modification in cells.

We next examined features of mitosis, counting mitotic spindles and assessing cells for micronuclei, structures produced by chromosome fragments or whole chromosomes that are not incorporated into the nucleus on cell division. SUMO conjugation promotes spindle assembly and chromosome segregation (Abrieu & Liakopoulos, 2019, Mukhopadhyay & Dasso, 2017), and as expected, depletion of SAE1/SAE2 increased multipolar mitotic spindles and the number of cells with micronuclei (Fig. 3 e-g). We found that WT-E1 and K164R-SAE2 complementation, but not C173G-SAE2 or K164Q-SAE2 expression, suppressed excessive micronuclei and multipolar spindles (Fig. 3 e-g), suggesting K164-SAE2 hypoacetylation promotes mitotic fidelity. Finally, as our *in vitro* analysis indicated K164-SAE2 is critical for SUMO1 selectivity when SUMO2 is present (Fig. 2d), we then tested the ability of overexpression of SUMO1 to improve mitotic defects in K164Q-SAE2 complemented cells. Indeed, expression of SUMO1 suppressed

multipolar spindles in K164Q-SAE2 expressing cells (Fig. 3h), consistent with the notion that deacetylation promotes SUMO1 isoform selectivity.

Discussion.

Here we show that the human SUMO activating enzyme is acetylated and deacetylated at K164-SAE2. *In vitro* K164Q, a near mimic of acetylation reduces the ability of the enzyme to activate SUMO1 over SUMO2 and alters the bias of SUMO paralogue conjugation. The SUMO E1 enzyme differs from all other small protein modifier activating enzymes in that it activates two related but different modifiers; SUMO1 shares only 50% similarity with SUMO2/3. Consistent with previous work from Walden *et al* 2003, suggesting the C-terminal regions of small modifier proteins are critical regions of distinction, we find that residue E93 of SUMO1 and Q89 of SUMO2 are part of the discrimination employed. The ability of the NEDD8 activating enzyme (APPBP1–UBA3) to discriminate between NEDD8 and ubiquitin (which are 55% identical) is mediated through similarly positioned residues in these small modifiers (Walden, Podgorski et al., 2003).

When the SUMO E1 is in the 'open confirmation' that promotes adenylation, the structures of SAE1:SAE2-SUMO-AVSN show that the SAE2-K164 ζ-nitrogen and SUMO1-E93 ε-carbonyl are 9.9 Å apart (Hann et al., 2019, Olsen et al., 2010). In contrast, when E1 is in its 'closed' state that promotes thioester bond formation, the ~4 Å separation between these residues could allow ionic interaction (Hann et al., 2019, Olsen et al., 2010) (Fig. 2e). As K164Q-SAE2 E1 alters isoform activation bias and also alters the equilibrium of isoform interactions in the absence of ATP, we speculate that both states are present in solution.

Deacetylation of acK164-SAE2 can be suppressed by HDAC6 inhibition. HDAC6 is one of the few HDACs found primarily in the cytoplasm, where it catalyses the removal of acetyl groups from substrates including α-tubulin and HSP90, and has been linked to microtubule dynamics (Boyault, Sadoul et al., 2007). As SUMO E1 is predominately nuclear, we speculate that the timing of acK164-SAE2 deacetylation may relate to nuclear envelop breakdown at the end of prophase in mitosis.

In *Sumo1* null mice, SUMO1 functions are compensated for by SUMO2 and SUMO3 (Zhang, Mikkonen et al., 2008). Our finding that K164Q-SAE2 suppresses SUMO1 conjugation and that SUMO1 overexpression supports mitosis in cells expressing the mutant suggest SUMO1 is the preferred paralogue for particular roles in mitosis that are not acutely compensated for by SUMO2/3. SUMO1-targets previously identified with the potential to regulate mitotic fidelity include BubR1 (Yang, Hu et al., 2012), NuMa (Seo, Kim et al., 2014), Aurora-A (Perez de Castro, Aguirre-Portoles et al., 2011), the RanBP2/RanGAP1*SUMO1/Ubc9 complex and its substrates (Flotho & Werner, 2012). Whether one, or all of these, are significant requires further investigation.

Our findings suggest that the ability to bias SUMO paralogue usage can be influenced through modification of the SUMO activating enzyme, which in turn is required for a subset of SUMO-regulated cellular functions. SAE1/SAE2 are heavily modified by post-translational modifications (e.g. (Elia, Wang et al., 2015)), suggesting further regulatory mechanisms are likely to be critical to the SUMO-system.

Acknowledgements: Grant funding. Wellcome Trust 206343/Z/17/Z (M.J, A.W, A.J.G), University of Birmingham (A.L). BBSRC: BB/V01983X/1, BB/S017283/1 BB/P009840/1 (TJK). Midlands Integrative Biosciences Training Partnership - BB/M01116X/1 (P.W. & B.F.C). We thank Jeremy Stark (City of Hope, Duarte U.S.A.) for U2OS DR-GFP and NHEJ-EJ5 cells and Annette Aichem (University of Konstanz, Switzerland) for the pGEX4T-3-FAT10 construct. We also thank the Microscopy and Imaging Services at Birmingham University (MISBU) and the UoB Flow Cytometry Services (UoBFC) in the Tech Hub facility for microscope and FACS support and maintenance.

Author contributions: A.K.W. (Immunofluorescence and analysis, DR-GFP and NHEJ-EJ5, Flag immunoprecipitations, Western blots); A.J.L (Site-directed mutagenesis, generation of stable cell lines, colony survival assays, acK164-SAE2

antibody development, protein overexpression and purification, *in vitro* SUMOylation assays, western blotting, structural analyses); M.J. (Protein expression and purification, *in vitro* activation of GST-tagged and untagged SUMO isoforms, NT647-labelling of WT E1 or K164Q-SAE2 E1, MST data analysis, western blotting, site-directed mutagenesis); A.J.G (siRNA and primer design, site-directed mutagenesis); P.W. and B.F.C. (MST sample measurement using Monolith NT.115 [NT.115Pico/N.T.LabelFree] instrument (NanoTemper Technologies). T.J.K Supervised P.W and B.F.C. J.R.M. supervised the project and wrote the paper. All authors wrote and edited the manuscript.

References.

Abrieu A, Liakopoulos D (2019) How Does SUMO Participate in Spindle Organization? *Cells* 8

Aichem A, Sailer C, Ryu S, Catone N, Stankovic-Valentin N, Schmidtke G, Melchior F, Stengel F, Groettrup M (2019) The ubiquitin-like modifier FAT10 interferes with SUMO activation. *Nat Commun* 10: 4452

Becker J, Barysch SV, Karaca S, Dittner C, Hsiao HH, Berriel Diaz M, Herzig S, Urlaub H, Melchior F (2013) Detecting endogenous SUMO targets in mammalian cells and tissues. *Nat Struct Mol Biol* 20: 525-31

Bhardwaj A, Das S (2016) SIRT6 deacetylates PKM2 to suppress its nuclear localisation and oncogenic functions. *Proc Natl Acad Sci U S A* 113: E538-47

Boyault C, Sadoul K, Pabion M, Khochbin S (2007) HDAC6, at the crossroads between cytoskeleton and cell signaling by acetylation and ubiquitination. *Oncogene* 26: 5468-76

Chang HM, Yeh ETH (2020) SUMO: From Bench to Bedside. *Physiol Rev* 100: 1599-1619

Chang PC, Izumiya Y, Wu CY, Fitzgerald LD, Campbell M, Ellison TJ, Lam KS, Luciw PA, Kung HJ (2009) Kaposi's sarcoma associated herpesvirus (KSHV) encodes a SUMO E3 ligase which is SIM-dependent and SUMO-2/3-specific. *J Biol Chem*

Desterro JM, Rodriguez MS, Kemp GD, Hay RT (1999) Identification of the enzyme required for activation of the small ubiquitin-like protein SUMO-1. *J Biol Chem* 274: 10618-24

Elia AE, Wang DC, Willis NA, Boardman AP, Hajdu I, Adeyemi RO, Lowry E, Gygi SP, Scully R, Elledge SJ (2015) RFWD3-Dependent Ubiquitination of RPA Regulates Repair at Stalled Replication Forks. *Mol Cell* 60: 280-93

Flotho A, Werner A (2012) The RanBP2/RanGAP1*SUMO1/Ubc9 complex: a multisubunit E3 ligase at the intersection of sumoylation and the RanGTPase cycle. *Nucleus* 3: 429-32

Gareau JR, Reverter D, Lima CD (2012) Determinants of small ubiquitin-like modifier 1 (SUMO1) protein specificity, E3 ligase, and SUMO-RanGAP1 binding activities of nucleoporin RanBP2. *J Biol Chem* 287: 4740-51

Garvin AJ, Morris JR (2017) SUMO, a small, but powerful, regulator of double-strand break repair. *Philos Trans R Soc Lond B Biol Sci* 372

Hann ZS, Ji C, Olsen SK, Lu X, Lux MC, Tan DS, Lima CD (2019) Structural basis for adenylation and thioester bond formation in the ubiquitin E1. *Proc Natl Acad Sci U S A* 116: 15475-15484

He X, Riceberg J, Soucy T, Koenig E, Minissale J, Gallery M, Bernard H, Yang X, Liao H, Rabino C, Shah P, Xega K, Yan ZH, Sintchak M, Bradley J, Xu H, Duffey M, England D, Mizutani H, Hu Z et al. (2017) Probing the roles of SUMOylation in cancer cell biology by using a selective SAE inhibitor. *Nat Chem Biol* 13: 1164-1171

Hendriks IA, Lyon D, Su D, Skotte NH, Daniel JA, Jensen LJ, Nielsen ML (2018) Site-specific characterisation of endogenous SUMOylation across species and organs. *Nat Commun* 9: 2456

Hendriks IA, Lyon D, Young C, Jensen LJ, Vertegaal AC, Nielsen ML (2017) Site-specific mapping of the human SUMO proteome reveals co-modification with phosphorylation. *Nat Struct Mol Biol*

Hendriks IA, Vertegaal AC (2016) A comprehensive compilation of SUMO proteomics. *Nat Rev Mol Cell Biol* 17: 581-95

Ilic D, Magnussen HM, Tirard M (2022) Stress - Regulation of SUMO conjugation and of other Ubiquitin-Like Modifiers. *Semin Cell Dev Biol*

Jochems J, Boulden J, Lee BG, Blendy JA, Jarpe M, Mazitschek R, Van Duzer JH, Jones S, Berton O (2014) Antidepressant-like properties of novel HDAC6-selective inhibitors with improved brain bioavailability. *Neuropsychopharmacology* 39: 389-400

Johnson ES, Blobel G (1997) Ubc9p is the conjugating enzyme for the ubiquitin-like protein Smt3p. *J Biol Chem* 272: 26799-802

Johnson ES, Schwienhorst I, Dohmen RJ, Blobel G (1997) The ubiquitin-like protein Smt3p is activated for conjugation to other proteins by an Aos1p/Uba2p heterodimer. *Embo J* 16: 5509-19

Joseph J, Liu ST, Jablonski SA, Yen TJ, Dasso M (2004) The RanGAP1-RanBP2 complex is essential for microtubule-kinetochore interactions in vivo. *Curr Biol* 14: 611-7

Joseph J, Tan SH, Karpova TS, McNally JG, Dasso M (2002) SUMO-1 targets RanGAP1 to kinetochores and mitotic spindles. *J Cell Biol* 156: 595-602

Kim SC, Sprung R, Chen Y, Xu Y, Ball H, Pei J, Cheng T, Kho Y, Xiao H, Xiao L, Grishin NV, White M, Yang XJ, Zhao Y (2006) Substrate and functional diversity of lysine acetylation revealed by a proteomics survey. *Mol Cell* 23: 607-18

Lois LM, Lima CD (2005) Structures of the SUMO E1 provide mechanistic insights into SUMO activation and E2 recruitment to E1. *Embo J* 24: 439-51

Meulmeester E, Kunze M, Hsiao HH, Urlaub H, Melchior F (2008) Mechanism and consequences for paralog-specific sumoylation of ubiquitin-specific protease 25. *Mol Cell* 30: 610-9

Mukhopadhyay D, Dasso M (2017) The SUMO Pathway in Mitosis. *Adv Exp Med Biol* 963: 171-184

Namanja AT, Li YJ, Su Y, Wong S, Lu JJ, Colson LT, Wu CG, Li SSC, Chen Y (2012) Insights into High Affinity Small Ubiquitin-like Modifier (SUMO) Recognition by SUMO-interacting Motifs (SIMs) Revealed by a Combination of NMR and Peptide Array Analysis. *Journal of Biological Chemistry* 287: 3231-3240

Okuma T, Honda R, Ichikawa G, Tsumagari N, Yasuda H (1999) In vitro SUMO-1 modification requires two enzymatic steps, E1 and E2. *Biochem Biophys Res Commun* 254: 693-8

Olsen SK, Capili AD, Lu X, Tan DS, Lima CD (2010) Active site remodelling accompanies thioester bond formation in the SUMO E1. *Nature* 463: 906-12

Perez de Castro I, Aguirre-Portoles C, Martin B, Fernandez-Miranda G, Klotzbucher A, Kubbutat MH, Megias D, Arlot-Bonnemains Y, Malumbres M (2011) A SUMOylation Motif in Aurora-A: Implications for Spindle Dynamics and Oncogenesis. *Front Oncol* 1: 50

Reverter D, Lima CD (2005) Insights into E3 ligase activity revealed by a SUMO-RanGAP1-Ubc9-Nup358 complex. *Nature* 435: 687-92

Rueden CT, Schindelin J, Hiner MC, DeZonia BE, Walter AE, Arena ET, Eliceiri KW (2017) ImageJ2: ImageJ for the next generation of scientific image data. *BMC Bioinformatics* 18: 529

Seo JS, Kim HN, Kim SJ, Bang J, Kim EA, Sung KS, Yoon HJ, Yoo HY, Choi CY (2014) Cell cycle-dependent SUMO-1 conjugation to nuclear mitotic apparatus protein (NuMA). *Biochem Biophys Res Commun* 443: 259-65

Tatham MH, Kim S, Jaffray E, Song J, Chen Y, Hay RT (2005) Unique binding interactions among Ubc9, SUMO and RanBP2 reveal a mechanism for SUMO paralog selection. *Nat Struct Mol Biol* 12: 67-74

Ulrich HD (2008) The fast-growing business of SUMO chains. *Mol Cell* 32: 301-5

Walden H, Podgorski MS, Huang DT, Miller DW, Howard RJ, Minor DL, Jr., Holton JM, Schulman BA (2003) The structure of the APPBP1-UBA3-NEDD8-ATP complex reveals the basis for selective ubiquitin-like protein activation by an E1. *Mol Cell* 12: 1427-37

Werner A, Flotho A, Melchior F (2012) The RanBP2/RanGAP1*SUMO1/Ubc9 complex is a multisubunit SUMO E3 ligase. *Mol Cell* 46: 287-98

Wienken CJ, Baaske P, Rothbauer U, Braun D, Duhr S (2010) Protein-binding assays in biological liquids using microscale thermophoresis. *Nat Commun* 1: 100

Wiryawan H, Dan K, Etuale M, Shen Y, Liao J (2015) Determination of SUMO1 and ATP affinity for the SUMO E1by quantitative FRET technology. *Biotechnol Bioeng* 112: 652-8

Yang F, Hu L, Chen C, Yu J, O'Connell CB, Khodjakov A, Pagano M, Dai W (2012) BubR1 is modified by sumoylation during mitotic progression. *J Biol Chem* 287: 4875-82

Zhang FP, Mikkonen L, Toppari J, Palvimo JJ, Thesleff I, Janne OA (2008) Sumo-1 function is dispensable in normal mouse development. *Mol Cell Biol* 28: 5381-90

Zhu J, Zhu S, Guzzo CM, Ellis NA, Sung KS, Choi CY, Matunis MJ (2008) Small ubiquitin-related modifier (SUMO) binding determines substrate recognition and paralog-selective SUMO modification. *J Biol Chem* 283: 29405-15

Zhu S, Goeres J, Sixt KM, Bekes M, Zhang XD, Salvesen GS, Matunis MJ (2009) Protection from isopeptidase-mediated deconjugation regulates paralog-selective sumoylation of RanGAP1. *Mol Cell* 33: 570-80

Figures and legends.

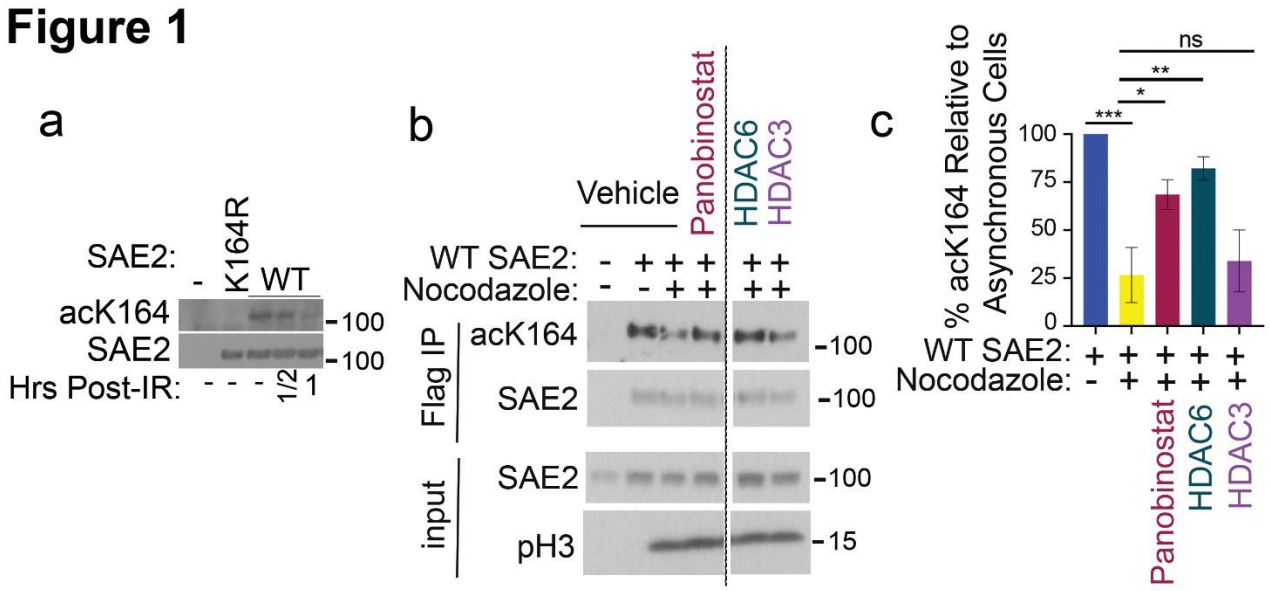

Figure 1. Acetylation of SAE2-K164.

a. Western blot analysis of acetyl-K164-SAE2 (mouse monoclonal) compared to anti-SAE2 of anti-FLAG immunoprecipitation from U2OS cells (- empty vector) and U2OS cells expressing FLAG-SAE2-K164R or WT FLAG-SAE2 and untreated or recovering from 10 Gy irradiation exposure.

b. Representative western blot of acetyl-K164-SAE2 (mouse monoclonal) following anti-FLAG immunoprecipitation from U2OS cells and U2OS cells expressing WT FLAG-SAE2 in unsynchronised cells and cells synchronised with nocodazole before releasing into mitosis for 10 mins. HDAC inhibitors were applied to cells in the last 2 hrs of nocodazole synchronisation at 2.5 µM and reapplied upon the release.

c. Quantification of the relative abundance of acetyl-K164-SAE2 relative to the total abundance of SAE2 immunoprecipitated. Error bars = SD; n=3. *** = $p< 0.001$, ** = $p< 0.01$, * = $p< 0.05$, ns= not significant $p>0.05$.

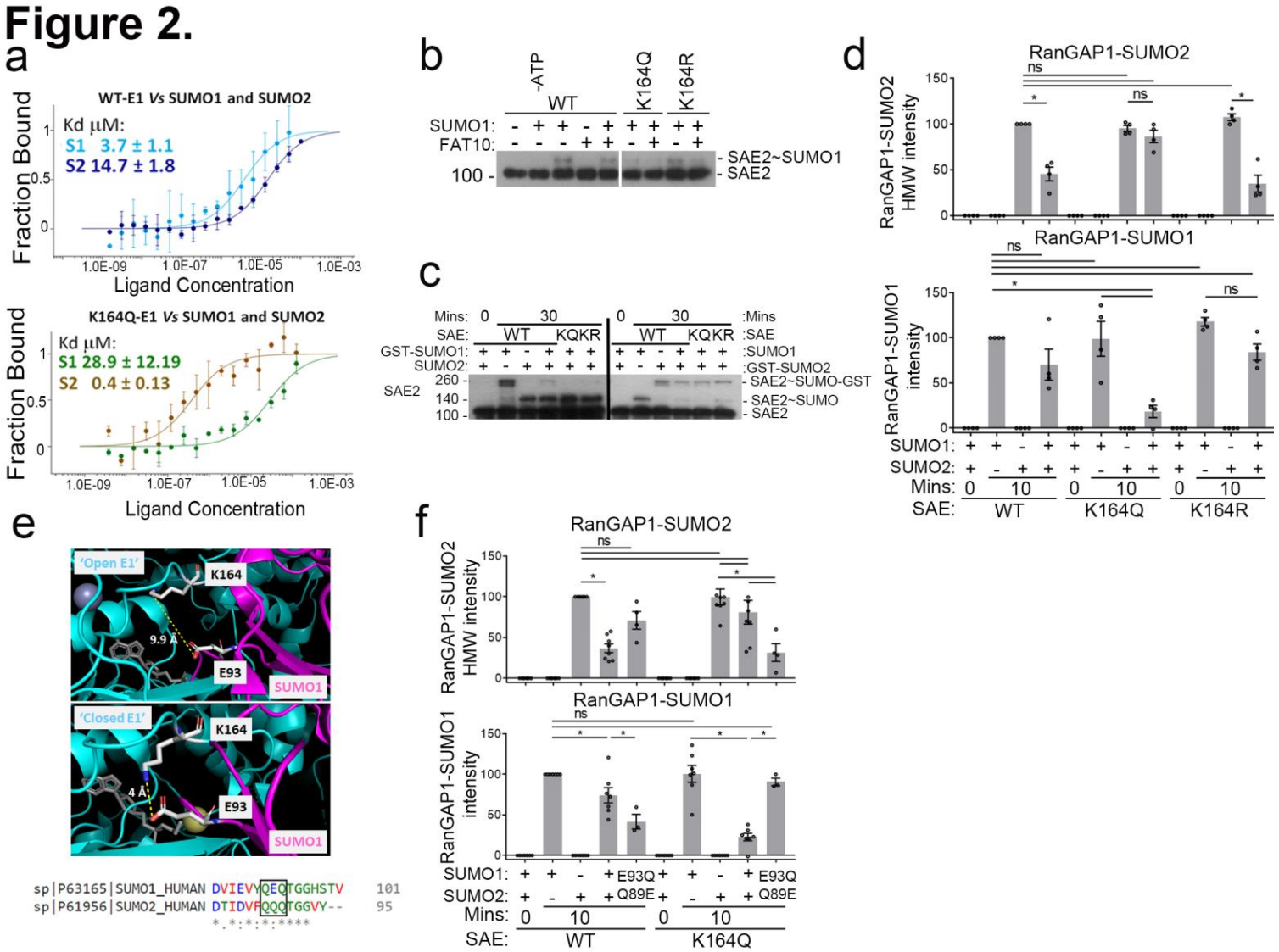

Figure 2. K164Q-SAE2 has an altered SUMO bias.

a. Altered SUMO isoform interactions. SUMO1 and SUMO2 concentrations from 125 µM down to 0.00381 µM were titrated against 10 nM of NT647-labeled, WT E1 (top) or K164Q-SAE2 E1 (bottom). Plotting of the change in thermophoresis and fitting of the data yielded a K_d of WT E1 with SUMO1 of 3.7 (±1.1) µM and with SUMO2 of 14.7 (±1.8) µM, the K_d of SAE2-K164Q E1 with SUMO1 was 28.9 (±12.2) µM and SUMO2 0.4 (±12.2) µM. Error bars = SD; n = 3.

b. *In vitro* SUMO1 activation by SAE1/SAE2 variants, assessed by loading of SUMO1 onto catalytic SAE2. *In vitro* SUMO1 activation by SAE1/SAE2 variants, assessed by loading of SUMO1 onto catalytic SAE2. Experiment comprises 1 µM SAE1/SAE2, 10 µM SUMO1, 5 mM ATP, and -/+ 10 µM FAT10. Reactions were started by the addition of ATP at 30 °C for 30 minutes and processed by non-reducing SDS-PAGE and αSAE2 western blot.

c. *In vitro* activation of GST-tagged and untagged SUMO isoforms (10 µM) by SAE1/SAE2 (200 nM) variants, as above in (**b**).

d. *In vitro* SUMOylation in presence of 20 µM SUMO1 and/or 20 µM SUMO2, 200 nM SAE1/SAE2, 500 nM UBC9, 10 µM RanGAP1, and 5 mM ATP, incubated at 30 °C for 10 minutes. Supp. Fig. 2b and c show analysis of band identities in SUMOylation assays. Error bars = SEM.; n = 4. Statistical significance was calculated using one-way ANOVA. *p<0.05.

e. Examination of human SUMO E1 K164-SAE2 (Cyan) in 'open' conformation (Top) with E93-SUMO1-AMSN (Magenta; PDB ID code 3KYC) and in the 'closed' conformation (Bottom) with E93-SUMO1-AVSN (Magenta; PDB ID code 3KYD; (Olsen et al., 2010)). Amino acid sequence alignment for SUMO1-E93 and SUMO2-Q89.

f. *In vitro* SUMOylation in presence of wild-type SUMO1, and/or SUMO2, E93Q-SUMO1 and Q89E-SUMO2 (all SUMO variants supplied at 20 µM), 200 nM SAE1/SAE2, 500 nM UBC9, 10 µM RanGAP1, and 5 mM ATP, incubated at 30 °C for 10 minutes. Error bars = SEM.; n = 4. Statistical significance was calculated using one-way ANOVA. *$p<0.05$.

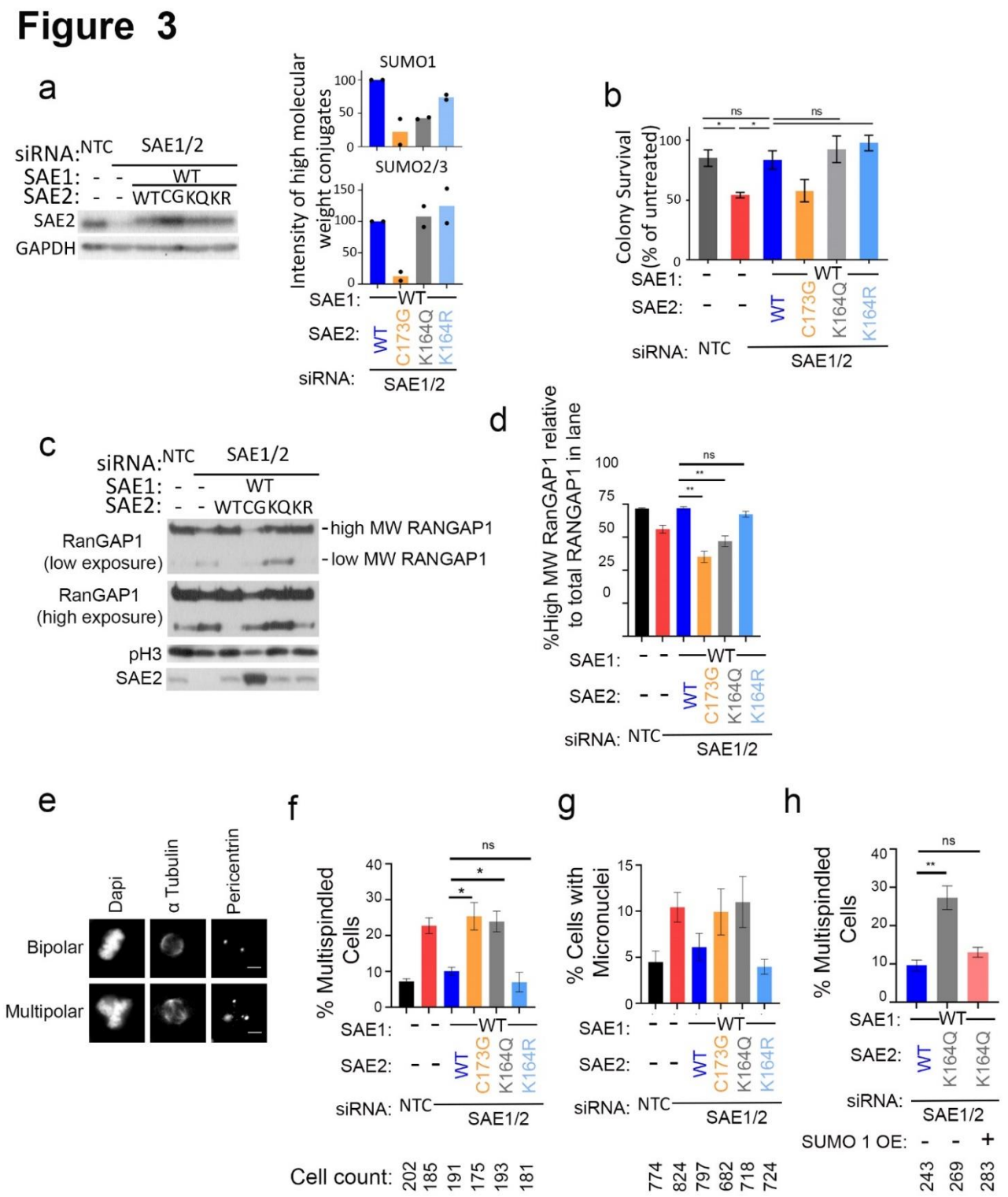

Figure 3. K164-SAE2 directs mitotic fidelity.

a. Western blot analysis (left) of SAE1/SAE2 depleted and complemented U2OS cells. Graphs (right) show quantification of the high-molecular weight SUMO1 and SUMO2/3 conjugates in cells complemented with the SAE2 variants shown. N=2.

b. U2OS depleted for SAE1/SAE2 and complemented with WT or SAE1/SAE2-mutants, subjected to 43 °C for 40 minutes before replating and counting after colony growth. Error bars = SD; n = 3. * = p≤ 0.05, ns = not significant p> 0.05.

c. Representative western blot depicting RanGAP1 and high molecular weight RanGAP1-SUMO1 after two sequential rounds of SAE1/SAE2 depletion and complementation in inducible U2OS stable cell lines synchronised in nocodazole and released for 5 mins into mitosis.

d. Quantification of the percentage of high molecular weight (SUMOylated) RanGAP1 relative to total RanGAP1 (high mw + low mw). Error bars SD; n = 3. **= p≤ 0.01, ns = not significant > 0.05.

e. Example images of cells bearing bipolar and multipolar spindles.

f. Quantification of laterally presented metaphase cells categorised as bipolar or multipolar. Presented as the percent of total cells counted with multipolar spindles, 35 mins after release from nocodazole. Error bars = SD; n = 3 independent repeats. * = p≤ 0.05, ns = not significant > 0.05.

g. Percent of cells complemented as shown with micronuclei. n = 3 independent repeats.

h. Quantification of the effect of SUMO1 overexpression in K164 acetyl-mimic cells. Laterally presented metaphase cells categorised as bipolar or multipolar. Presented as the percent of total cells counted with multipolar spindles, 35 mins after release from nocodazole. Error bars SD; n = 3 independent repeats. **= p≤ 0.01, ns = not significant > 0.05.

Supplemental Figures

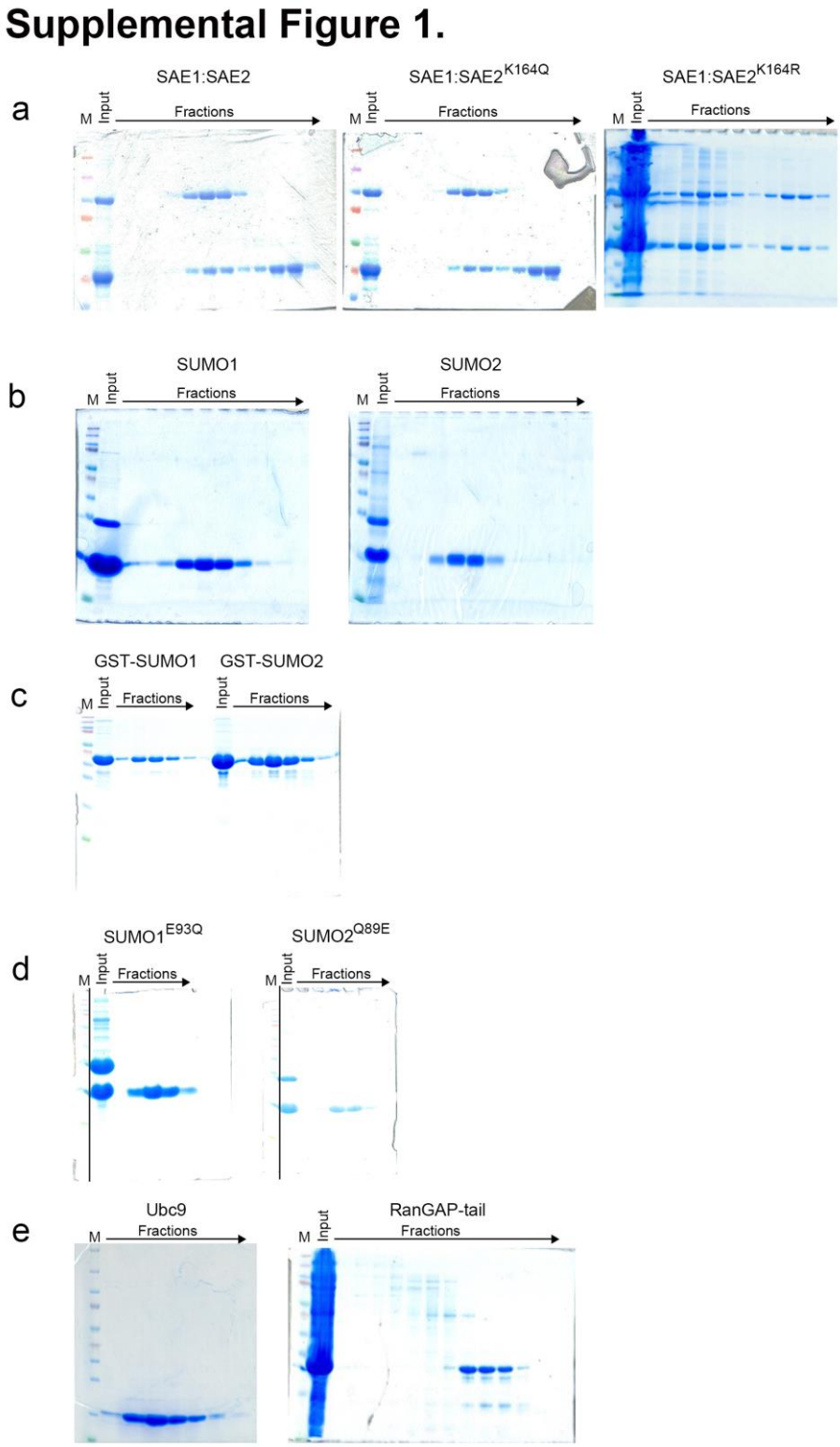

Supplemental Figure 1.

Representative Instantblue stained SDS-PAGE gels from SEC fractions for the respective purified proteins. Shown here are gels from (**a**) WT SAE1/SAE2, SAE1/SAE2-K164Q, and SAE1/SAE2-K164R; (**b**) WT SUMO1 and SUMO2; (**c**) GST-SUMO1 and GST-SUMO2; (**d**) SUMO1-E93Q and SUMO2-Q89E; and (**e**) UBC9 and RanGAP1-tail purification.

Supplemental Figure 2

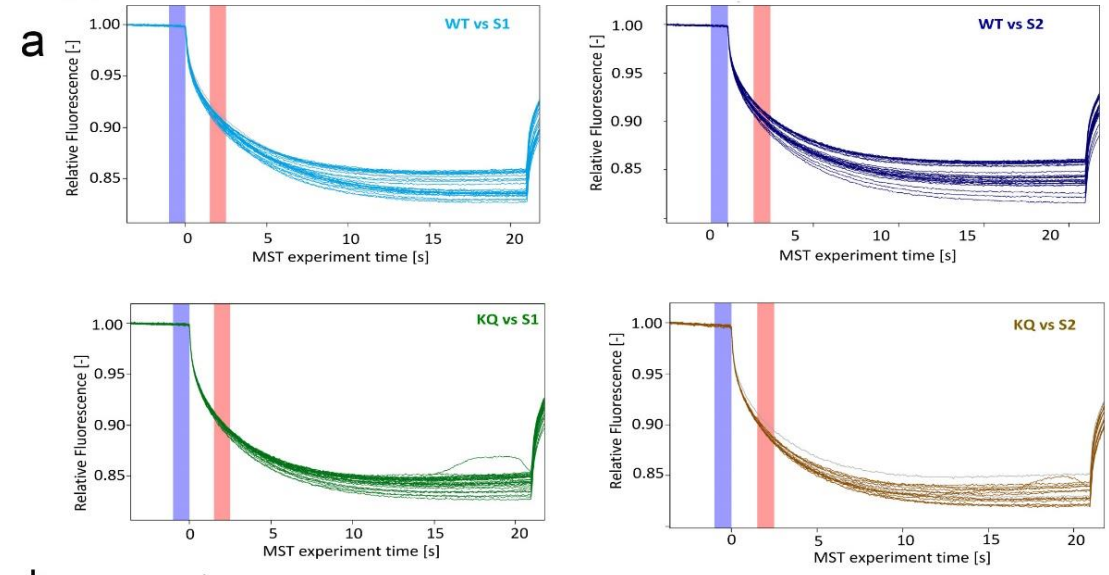

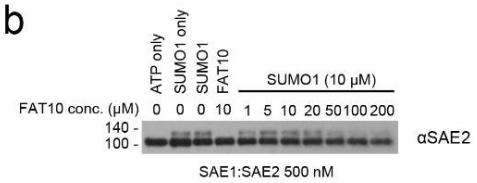

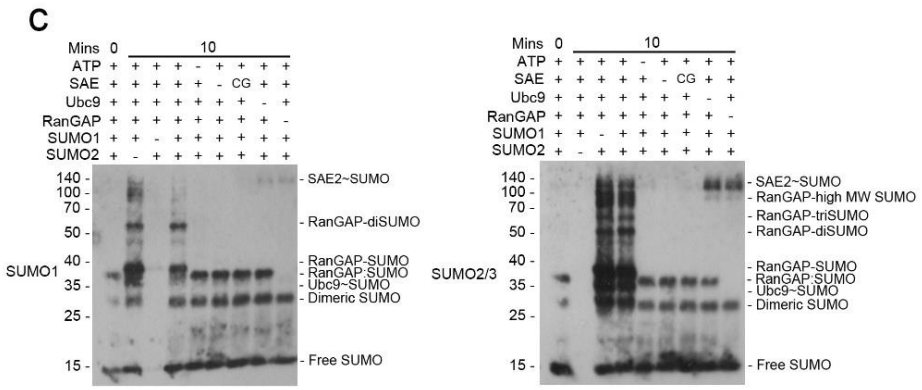

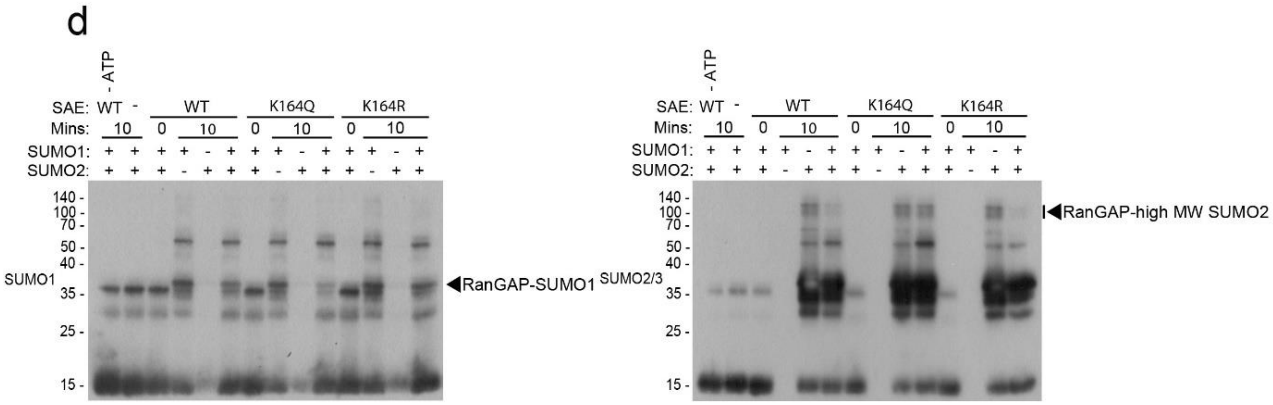

Supplemental Figure 2.

- **a.** MST Thermographs of SUMO1 or SUMO2 binding to WT or K164Q-SAE2 E1 provide well-defined curves. The cold region is set to 0 s (blue) and the hot region set to 2.5 s (red) to determine the K_d of the interaction and to avoid any potential convection phenomena.
- **b.** *In vitro* SUMO1 activation by SAE1/SAE2 was assessed by loading of SUMO1 onto catalytic SAE2. The experiment comprises: 1 µM SAE1/SAE2, 10 µM SUMO1, 5 mM ATP, and increased µM FAT10. Reactions started on the addition of ATP at 30 °C for 30 minutes and processed by non-reducing SDS-PAGE and αSAE2 western blot.
- **c.** *In vitro* RanGAP1 SUMOylation control blots for SUMO1 and SUMO2/3. The first condition contains all reaction components but was not incubated at 30 °C and gives 3 distinct bands, taken as unconjugated SUMO (15 kDa), dimeric SUMO (30 kDa), RanGAP1:SUMO (37 kDa). These bands persist on incubation at 30 °C for 10 mins in conditions which omit ATP, SAE1/SAE2, UBC9, and in the use of the catalytically inactive SAE1/SAE2-C173G (CG). The 37 kDa band is absent in the omission of RanGAP1 in the αSUMO1 and αSUMO2/3 blots, indicative of a SUMO-E1-E2-independent RanGAP1:SUMO species. SAE2~SUMO is dependent on ATP, SAE1/SAE2 with catalytic activity and therefore accumulates in conditions –Ubc9 and –RanGAP1. RanGAP1-SUMO formation is dependent on all SUMOylation assay components, including incubation at 30 °C, as is the formation of RanGAP1-polySUMO, which is most prominent in the αSUMO2/3 blot. Omission of SUMO protein isoform controls abrogates the signal, indicating that the antibodies are isoform-specific.
- **d.** Representative blots for the *in vitro* SUMOylation data in Fig. 2d. Reactions comprised 20 µM SUMO1 and/or 20 µM SUMO2, 200 nM SAE1/SAE2, 500 nM UBC9, 10 µM RanGAP1, and 5 mM ATP, incubated at 30 °C for 10 minutes. Conditions were processed by SDS-PAGE in duplicate such that western blots were developed using αSUMO1 and αSUMO2/3 antibodies. Note that the bands indicated are those quantified.

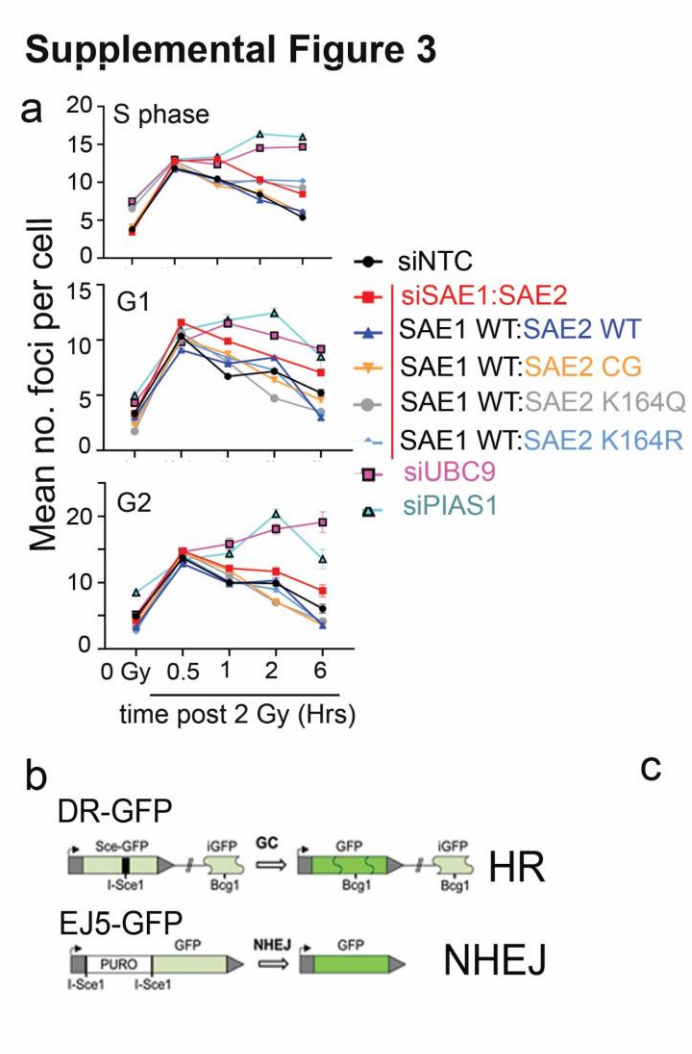

	Number of cells analysed							
	siNTC	siSAE1:SAE2					siUBC9	siPIAS1
	-	-	SAE1 WT: SAE2 WT	SAE1 WT: SAE2 CG	SAE1 WT: SAE2 K164Q	SAE1WT: SAE2 K164R	-	-
S phase								
0 Gy	2185	2142	2209	2994	2179	3064	1546	1355
0.5 hr	3430	3412	3208	3381	3394	3193	1641	1780
1 hr	3286	3466	3074	3082	1099	2720	1419	1347
2 hr	3417	3205	1051	2776	2420	3272	1507	1467
6 hr	3279	2952	2444	2452	2042	3075	1402	1259
G1								
0 Gy	2385	2750	2119	1841	766	1623	615	904
0.5 hr	1151	1111	1256	1153	847	1335	580	447
1 hr	708	1301	1604	1598	1025	989	405	424
2 hr	1069	910	1247	1284	998	1104	418	347
6 hr	461	647	887	811	779	782	227	104
G2								
0 Gy	931	890	546	471	264	379	264	589
0.5 hr	342	339	417	265	311	468	174	224
1 hr	421	313	300	440	346	219	145	264
2 hr	427	217	406	302	223	293	129	178
6 hr	156	128	184	205	223	185	55	98

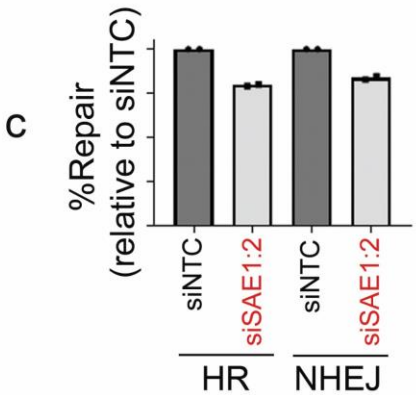

Supplemental Figure 3.

a. Quantification of γH2AX foci in cells treated with the siRNAs shown and complemented or not with SAE2 variants. siUBC9 and siPIAS1 are used for comparison. Results displayed for data isolated from S phase (top), G1 (middle) and G2 (bottom) cell populations. The number of cells analysed for each of the data points is displayed in the table to the right.

b. Illustration of the integrated DNA repair substrates for homologous recombination (top) and non-homologous end-joining (bottom).

c. U2OS cells bearing integrated DNA repair read-outs and treated with NTC or siSAE1/siSAE2 and transfected with the enzyme, I-SCE-1. n = 2.

Materials and Methods.

acK164-SAE2 Antibody Generation. Custom mouse monoclonal (clone 30E2-2) was raised against acetylated K164-SAE2 peptide (HP{Lys-Ac}PTQRTFPGC) by GenScript. Available on request to the corresponding author subject to completion of an M.T.A.

FLAG immunoprecipitation. U2OS cultured at 37 °C/5% CO_2 in 15 cm^2 dishes supplemented with 4 µg/ml Doxycycline *(*Sigma*)* for 48 hours to induce exogenous SAE1/SAE2 expression. Cells washed with 1 ml ice-cold TBS (20 mM Tris/HCl pH 7.5, 150 mM NaCl) before suspension in RIPA Buffer (50 mM Tris-HCl pH 7.5, 150 mM NaCl, 1% TritonX100, 0.25% Sodium deoxycholate, 0.1% SDS, 1 mM EDTA, 10 mM NaF) plus EDTA-free protease inhibitor cocktail (Roche) and PhosSTOP (Roche). Lysis mix incubated on ice for 10min and sonicated at 50% intensity for 10s. Samples were centrifuged at 14,000xg/4 °C for 10 mins, and supernatant combined with 15 µl FLAG(M2) agarose (Sigma), incubated with mixing O/N at 4 °C IP samples were centrifuged at 1,000xg/4 °C for 2min to pellet FLAG beads. Supernatant discarded and beads washed with TBST. 30 µl 4xSDS loading buffer was added to beads with boiling at 95°C for 10 mins and centrifuged at 5,000xg/RT to pellet beads. For synchronising cells in mitosis, 100 ng/ml nocodazole was added to relevant dishes at 48 hrs after SAE1/SAE2 induction and left for 17 hrs. HDAC inhibitors were applied to synchronising cells 15 hours into Nocodazole treatment at 2.5 µM for 2 hours. At 17 hours cells were washed twice with PBS and released into mitosis for 10 minutes. Cells were then harvested via mitotic shake off and lysed as above in ice-cold RIPA Buffer (50 mM Tris-HCl pH 7.5, 150 mM NaCl, 1% TritonX100, 0.25% Sodium deoxycholate, 0.1% SDS, 1 mM EDTA, 10 mM NaF) plus EDTA-free protease inhibitor cocktail (Roche) and PhosSTOP (Roche) supplemented with 2 µM Panobinostat.

Western blotting. For a list of antibodies, see Supp. Table 5. Samples were subject to SDS-PAGE and transferred onto Immobilon-P PVDF-membrane (Merck). Membranes were blocked in 5% milk in PBST or in 5 % BSA with TBST for 30mins. Incubation with primary antibodies for 16 hours/4 °C/rolling. Membranes washed in PBST/TBST for 3x10mins and then incubated with relevant secondary HRP antibodies in blocking solution for minimum 1 hour/RT. Membranes washed in PBST/TBST for 3x10mins and HRP stimulated with EZ-ECL mix (Biological Industries) or ECL Prime (Amersham). Blots exposed to X-ray film (Wolflabs) and developed with KONICA MINOLTA SRX-101A. Densitometry calculations performed using Image J.

Generation of plasmids. See Supp. Table 1 for a comprehensive list of the vectors used. The SAE2-T2A-SAE2 pcDNA5/FRT/TO construct was designed by AJG and generated by GenScript using KpnI and NotI restriction sites. pET28a-SAE1 was cloned using NheI and BamHI restriction sites; pET28b-SAE2 was cloned using NcoI and NheI; pET23a-Ubc9 was cloned using NdeI and BamHI; and pET23a-RanGAP1 was made using NdeI and BamHI restriction sites. pGEX4T-1-SUMO1-3 was designed by AJG and made by GenScript by cloning SUMO1-3 cDNA into BamHI and EcoR1 restriction sites. pGEX4T-3-FAT10 construct was a generous gift from Dr. Annette Aichem

Protein overexpression and purification. BL21 (DE3; NEB) were transformed with the relevant plasmids (Supp. Table 1). Starter cultures were established by inoculating 40 ml LB (Melford; Kan 50 µg/ml or Amp 100 µg/ml) with a single colony, grown O/N at 37 °C. 10 ml starter culture used to inoculate each litre LB (Kan 50 µg/ml or Amp 100 µg/ml) and grown at 37 °C/180 rpm to OD_{595} ~0.6. Protein overexpression induced with (isopropyl-β-D-thiogalactoside) IPTG and temperature adjusted as follows, SUMO1 and SUMO2 at 0.5mM IPTG/18 °C/18 hours; SAE1 and SAE2 at 1 mM IPTG/25 °C/6 hours; UBC9 at 1 mM IPTG/37 °C/4 hours; RanGAP1-tail (aa398-587) at 1 mM IPTG/37 °C/4 hours; and FAT10 at 0.1 mM IPTG/25 °C/5 hours, with shaking at 180 rpm. Overexpression protocols for SAE1/SAE2, UBC9, and RanGAP1 were adapted from Flotho *et al.*, 2012 (Flotho & Werner, 2012) and for FAT10 (Aichem et al., 2019). BL21(DE3) cells were harvested by centrifugation at 5,000xg/4 °C/10min with resulting pellet resuspended in 10 ml cold lysis buffer (20 mM Tris-HCl pH8, 130 mM NaCl, 1mM EGTA, 1mM EDTA, 1% Tritonx100, 10% Glycerol, 1 mM DTT, EDTA-free protease inhibitor (*Roche*)). Separately overexpressed SAE1 and SAE2 combined here. 0.5 mg/ml lysozyme was added and incubated for 30 mins/4 °C/rolling. 1 U/ml DNase (Thermo Fisher) added before sonication at 5x30s at 100% intensity with 2-min recovery – all on ice. Samples were centrifuged at 48,000xg/4 °C/30 mins in a JLA-25.50 and supernatant was filtered through a 0.45 µm PES membrane (Millex) and combined protein-tag-specific resin. Prior to use resins were washed twice in PBS and once in the lysis buffer, with centrifugation performed at 1,000xg/4 °C/3 mins. Respective protein purification continued as follows.

SUMO1, SUMO2, and FAT10 purification. GST-SUMO1/SUMO2 and GST-FAT10 were combined with 250 µl glutathione Sepharose 4B beads (Cytvia) and incubated for 3 hours/4 °C/rolling. Beads were centrifuged at 1,000xg/4 °C/10 mins with supernatant collected. Wash steps comprised 3x10 ml lysis buffer suspension of beads and 1x10 ml cleavage buffer (20 mM Tris-HCl pH 8.4, 150 mM NaCl, 1.5 mM $CaCl_2$) with centrifugation as above. Beads were then suspended in 500 µl cleavage buffer supplemented with 16 U Thrombin cleaving protease and incubated at 4 °C/16 hours/rolling. Samples were then centrifuged at 1,000xg/4 °C/3 minutes and the supernatant collected for centrifugation at 14,000xg/4 °C/20 mins to clear any beads or aggregate. The 500 µl sample was subjected to size-exclusion chromatography (SEC) through an AKTA pure™ (UNICORN™ software) Superdex200 Increase 10/300 GL column equilibrated in 20 mM Hepes pH 7.5, 100 mM NaCl, 0.5 mM TCEP: 0.5 ml fractions collected. Fractions constituting a UV_{280} trace peak were analysed by SDS-PAGE stained with InstantBlue (Lubioscience; Supp. Fig. 1b-e). Pure protein fractions were pooled and stored at -80 °C. See Supp. Table 2.

Ubc9 purification. Column filled with 10 ml SP-Sepharose beads and 60 ml UBC9 lysate applied at ~1 ml/min; FT collected and reapplied. UBC9 lysis buffer was passed through a column for wash step. 20 ml UBC9 elution buffer (50 mM Na-phosphate pH 6.5, 300 mM NaCl, 1 mM DTT, 1 cOmplete protease inhibitor (EDTA-free) tablet/50 ml) applied to beads and 1.5 ml fractions collected - 10 µl samples analysed by 15% SDS-PAGE and InstantBlue stain. Fractions with the greatest quantity and purity of UBC9 protein combined and concentrated down to 5 ml using 3-kDa MWCO centrifugal concentrator (Thermo Scientific) at 4,000xg/4 °C. Sample cleared by centrifugation at 14,000xg/4 °C/20 mins before SEC through a Superdex75 equilibrated in transport buffer (20 mM Hepes pH 7.3, 110 mM potassium acetate, 1 mM EGTA, 1 mM DTT, 1 cOmplete protease inhibitor tablet/L): 4 ml fractions collected. Fractions constituting UV_{240} peak were analysed by 15% SDS-PAGE and Instantblue stain. Pure UBC9 protein fractions (Supp. Fig. 1e) were pooled and concentrated as before, and finally aliquoted and stored at -80 °C. See Supp. Table 2

SAE1/SAE2 and RanGAP1-tail purification. These His-tagged protein lysates were combined with 1 ml nickel beads (Sigma) and incubated at 4 °C/2 hours/rolling. Samples were then centrifuged at 1,000xg/4 °C/10 mins to pellet nickel beads; FT collected and retained. Nickel-bead:His-protein pellet suspended in 10 ml wash buffer ahead of centrifugation as before; supernatant retained. Nickel beads resuspended in 5 ml elution buffer and centrifuged as before; supernatant extracted and pushed through 0.45 µm PES filter. This protein suspension was run using an AKTA pure™ (UNICORN™ software) on a HiLoad 16/600 Superdex200 pg column equilibrated with 20 mM Hepes pH 7.5, 100 mM NaCl, 0.5 mM TCEP buffer: 2 ml fractions collected. Fractions corresponding with a UV_{280} peak were analysed by SDS-PAGE stained with InstantBlue. Fractions containing the purest SAE1/SAE2 or RanGAP1 (Supp. Fig. 1a & e) were pooled and exposed to 4,000xg/4 °C in centrifugal concentrators with 30 kDa and 10 kDa MWCO, respectively. Proteins were aliquoted and stored at -80 °C. See Supp. Table 2.

Microscale thermophoresis (MST). SAE1/SAE2 was labelled using Protein Labelling Kit RED-NHS 2nd Generation (NanoTemper Technologies). The labelling reaction was performed according to the manufacturer's instructions in the supplied labelling buffer, applying a concentration of 20 µM protein (molar dye: protein ratio ≈ 3:1) at RT for 30 min in the dark. Unreacted dye was removed with the supplied dye removal column equilibrated with MST buffer (20 mM Hepes pH 8.35, 150 mM NaCl, 0.5 mM TCEP). The degree of labelling was determined using UV/VIS spectrophotometry at 650 and 280 nm. A degree of labelling of 0.5-0.6 was typically achieved. The labelled SAE1/SAE2 protein was adjusted to 20 nM with MST buffer supplemented with 0.005% Tween20. The SUMO1/SUMO2 ligand was dissolved in MST buffer supplemented with 0.005% Tween20, and a series of 16 1:1 dilutions was prepared using the same buffer, producing ligand concentrations ranging from 125 mM to 0.00381 µM. For the measurement, each ligand dilution was mixed with one volume of labelled SAE1/SAE2 protein for a final concentration of 10 nM and final ligand concentrations ranging from 125 mM to 0.00381 µM. After 10min, incubation samples were centrifuged at 10,000xg for 10 mins, and loaded into Monolith NT.115 [Premium] Capillaries (NanoTemper Technologies). MST was measured using a Monolith NT.115 [NT.115Pico/N.T.LabelFree] instrument (NanoTemper Technologies) at an ambient temperature of 22 °C. Instrument parameters were adjusted to 20% LED. power and high [low/medium] MST power. Data of three independently pipetted measurements were analysed (MO.Affinity Analysis software version 2.3, NanoTemper Technologies) using the signal from an MST-on time of 2.5s.

SUMOylation assays. All proteins were diluted in SUMO assay buffer (SAB; 20 mM Hepes, 50 mM NaCl, 5 mM $MgCl_2$) and quantified on a NanoDrop2000/2000c (Thermo Fisher Scientific), using SAB to adjust proteins to target concentrations as in Supp. Table 2. Reaction mixes prepared to V_T 20 µl SAB with 200 nM SAE1/SAE2, 500 nM UBC9,

10 µM RanGAP1, 20 µM SUMO1, and 20 µM SUMO2. The reaction was started by addition of 5 mM ATP with incubation at 30 °C for 10 mins, and reactions were terminated by addition of 20 µl 4xLoading buffer (reducing-agent free) and incubation of samples at 95 °C for 10 mins. Samples were centrifuged at 14,000 xg/5 mins ahead of processing by SDS-PAGE and western blot analysis.

SAE1/SAE2-loading assays. Experiments conducted as above in V_T 20 µl SAB containing 1 µM SAE1/SAE2 and 10 µM SUMO1 and SUMO2; reaction started on addition of 5 mM ATP and incubation at 30 °C for 30min. Where applicable FAT10 was added at 10 µM. The reaction was terminated with 20 µl 4xLoading buffer (reducing-agent free) and incubated at 95 °C. Samples were processed by SDS-PAGE and western blotting for SAE2.

Site-Directed Mutagenesis. Primers were designed for mutagenesis (Supp. Table 3), with mutagenesis performed by PCR using PfU (Promega). All mutagenesis was confirmed by Sanger Sequencing (Source Bioscience).

Tissue culture. Parental FlpIn™ U2OS cells were obtained from Morris Lab cells stocks and grown in Dulbecco's Modified Eagle Media (DMEM) supplemented with 10% Fetal Bovine Serum (FBS) and 1% Penicillin/Streptomycin. Cells were cultured in Corning T75 flasks and 10 cm^2 plates and kept at 37 °C and 5% CO_2. Once cells reached 70-80% confluency, they were passaged. Cells were tested for Mycoplasma by Hoescht staining. Cell lines have not been authenticated.

Inducible stable cell line generation. U2OS^{TrEx}-Flp-In™ (a gift from Grant Stewart, University of Birmingham) were co-transfected with SAE2-T2A-SAE1 cDNA in the pcDNA5/FRT/TO vector and the Flp-recombinase cDNA in the pOG44 vector at a 5:1 pcDNA5/FRT/TO DNA: pOGG44 DNA ratio using FuGene6 (Roche) at a ratio of 4:1 FuGene (µl): DNA (µg). Blank control transfections were performed as a control for selection. Two days after transfection, cells were selected with 150 µg/ml Hygromycin (Thermo Fisher Scientific) with culture medium replaced every 2-3 days; selection exerted for ~2 weeks. After selection, cells were expanded and tested for expression of siRNA-resistant HA-SAE1/FLAG-SAE2 through treatment with siSAE1/siSAE2 (5 nM each) and 4 µg/ml Doxycycline for 72-hours. Cell lysates were prepared in 4xSDS loading buffer and western blot analysis performed.

Plasmid and siRNA transfection. FuGene6 (Roche) was used at 2:1 FuGene (µl): DNA (µg), following the manufacturer's guidelines. siRNA transfections were carried out using the transfection reagent Dharmafect1 (Dharmacon) following the manufacturer's instructions. For a full list of siRNA sequences, see Supp. Table 4.

Immunofluorescent staining. The staining for γH2AX foci kinetics was performed as follows. Cells were plated directly onto 48 well plates at 1 x 10^4 cells/ml and treated with siRNA for 72 hours, complemented with SAE1/SAE2 variants by addition of 4 µg/ml Doxycycline. Prior to 2 Gy irradiation cells were pulsed with 1 µM EdU for 10 mins. 0 Gy samples were fixed directly after Edu for 5 mins at 37 °C and 5% CO_2. After irradiation cells were allowed to recover for allotted timepoints before pre-permeabilisation with CSK buffer (100 mM NaCl, 300 mM sucrose, 3 mM $MgCl_2$, 10 mM PIPES pH 6.8) for 1 minute before fixation with 4 % PFA Once fixed the cells were permeabilised for a further 5 mins using 0.5% Triton X100 in PBS before incubation with blocking solution - 10% FCS in PBST for 30 mins. EdU was labelled by Click-iT® chemistry according to the manufacturer's protocols (Life Technologies) with Alexa-647-azide. Cells were washed then blocked for a further 30 mins before incubation with primary antibody in 10% FCS PBST. See Supp. Table 6 for a list of antibodies. Cells were washed in PBST before incubation with secondary antibody. Cells were then washed three times in PBS and the DNA stained using Hoescht at a 1:50,000 concentration for 5 mins. Excess of Hoescht was washed with PBS before antibodies were fixed in place by a 5 min PFA fix. PBS was reapplied to cells and imaging proceeded within 3 days. Cells for micronuclei and mitotic spindle staining were plated at 2 x 10^4 cells/ml in 24 well plates on glass coverslips and treated with siRNA and Doxycycline as described above. Micronuclei samples were fixed 72 hours later with 4% PFA before DNA staining using Hoescht. Coverslips were mounted onto Snowcoat slides using Immunomount. Mitotic spindle samples were treated with 100ng/ml Nocodazole 48 hr after siRNA and Doxycycline addition and incubated for a further 16 hrs. Media was then removed, and cells washed twice in PBS. Media supplemented with Doxycycline was added to cells, which were allowed to progress through mitosis for 35 mins before fixation with PFA. Cells were permeabilised for 5 mins using 0.5% Triton X100 in PBS and blocked in 10% FCS in PBST for 1hr before the addition of primary antibodies. See Supp. Table 6 for a list of antibodies. Samples were washed in

PBST before the addition of secondary antibodies. DNA was stained with Hoescht and coverslips were mounted onto glass slides. All primary and secondary antibodies were incubated for 1hr RT

Microscopy and analysis. High content γH2AX foci imaging and analysis was conducted using the CellInsight CX5 HCS Platform with 20x objective lens using Compartmental Analysis BioApplication software. Raw data outputs from this analysis were then extracted so that cell cycle positioning could be performed plotting the total nuclear intensity of the Hoescht signal against the log average nuclear intensity of the EDU. signal. This was then used to discriminate the foci numbers of γH2AX in S phase, G1 and G2. All other staining was imaged using the Leica DM6000B microscope using an HBO lamp with 100W mercury short arc UV bulb light source and four filter cubes, A4, L5, N3 and Y5, which produce excitations at wavelengths 360, 488, 555, and 647 nm, respectively. To analyse micronuclei, all cells were counted in at least 4 fields of view, and a minimum of 150 cells were counted per condition per experimental repeat. Mitotic spindles were assessed by counting all laterally presented metaphase cells in a field of view, with a minimum of 50 cells counted per condition experimental repeat.

Colony survival assays. U2OS Flp-In™ cells were plated in 24-well plates at $2x10^4$/ml and treated with siSAE1/siSAE2 (5 nM each) and Dox for 72 hours. Cells were heat shocked in a water bath at 43 °C for 40 mins with control condition placed in a 37 °C water bath. Cells were suspended in 100 µl 1xTrypsin followed by 900 µl DMEM and plated at limiting dilutions in 6-well plates. Plates were incubated for 7 days at 37 °C and 5% CO_2, then stained with 0.5% crystal violet (50% methanol) and counting.

Densitometry. Densitometry was calculated using ImageJ (Rueden, Schindelin et al., 2017) to quantify western blot band intensities. All quantification is from at least 3-independent experiments. To quantify RanGAP1-SUMO from *in vitro* assay western blots, band intensities were measured, and the background was subtracted. Values were normalised against the WT SAE1/SAE2:SUMO1/2-only condition RanGAP1-SUMO intensity. For the densitometry to calculate the levels of SUMO conjugation, we calculated the relative amounts of SUMO 'smear' in cells using densitometry with Image J. The amount was then normalised to a GAPDH loading control.

DR-GFP and NHEJ-EJ5. U2OS-DR3-GFP and NHEJ-EJ5 (reporter cell lines) were a generous gift from Jeremy Stark (City of Hope, Duarte U.S.A.). U2OS reporter cell lines were simultaneously co-transfected with siRNA using Dharmafect1 (Dharmacon) and DNA (RFP and *I-Sce1* endonuclease expression constructs) using FuGene6 (Promega), respectively. After 16 hours, the media was replaced and cells were grown for a further 48-hour before fixation in 2% PFA, RFP and GFP double-positive cells were scored by FACS analysis using a CyAn flow cytometer and a minimum of 10,000 cells counted. Data was analysed using Summit 6.2 software. The percentage of GFP-RFP positive cells was determined as a fraction of the total RFP (RFP only +double GFP-RFP).

Statistics and Reproducibility. All statistics were done using two-sided unpaired t-test or one-way ANOVA analysis. Significance shown as *$p<0.05$, **$p<0.01$, ***$p<.0.001$, n.s = not-significant $p>0.05$. All experiments were repeated to generate biological replicates. The n-value is reported for each experiment.

Supplemental Tables

Supplemental Table 1 Vectors, gene(s) of interest encoded, and antibiotic resistance

Vector	Protein encoded	Tag	Antibiotic resistance
pcDNA5/FRT/TO	SAE2-T2A-SAE1	FLAG- and HA, resp.	Ampicillin/Hygromycin
pET28a	SAE1	Hexa-His	Kanamycin
pET28b	SAE2	Hexa-His	Kanamycin
pET23a	Ubc9	-	Ampicillin
pCDNA5/FRT/TO	SUMO1	myc-His SUMO1	Ampicillin
pGEX4T-1	SUMO1-3	GST	Ampicillin
pET23a	RanGAP1-tail (aa398-587)	His	Ampicillin
pGEX4T-3	FAT10	GST	Ampicillin

Supplementary Table 2 - Recombinant proteins and their parameters

Protein	Molecular weight (kDa)	Extinction coefficient (ε/1000) -Cys reduced-	Useful target concentration (mg/ml)
SAE1:SAE2	109.655	69.330	0.200
Ubc9	18.007	29.700	0.150
RanGAP1 (aa398-587)	22.386	10.805	4.500
SUMO1	11.277	4.470	2.000
GST-SUMO1	39.594	47.330	2.500
SUMO2	10.753	1.490	2.000
GST-SUMO2	39.099	44.350	2.500
SUMO4	10.839	2.980	2.000
Ubiquitin	8.565	1.490	4.000
FAT10	18.617	11.710	7.000

Supplementary Table 3 - Oligonucleotide primers used for cloning and site-directed mutagenesis

Gene	Cloning & Mutagenesis Primers	Primer Sequence
SAE2	C173G_F	GAGAACCTTTCCTGGCGGTACAATTCGTAACAC
	C173G_R	GTGTTACGAATTGTACCGCCAGGAAAGGTTCTC
	K164Q_F	GTTATGAGTGTCATCCTCAGCCGACCCAGAGAAC
	K164Q_R	GTTCTCTGGGTCGGCTGAGGATGACACTCATAAC
	K164R_F	GTGTTATGAGTGTCATCCTAGGCCGACCCAGAGAACCTTTC
	K164R_R	GAAAGGTTCTCTGGGTCGGCCTAGGATGACACTCATAACAC
SUMO1	E93Q_Fwd	AGTTTATCAGCAACAAACGGG
	E93Q_Rev	CCCGTTTGTTGCTGATAAACT
SUMO2	Q89E_Fwd	GTGTTCCAAGAGCAGACGG
	Q89E_Rev	CCGTCTGCTCTTGGAACAC

Supplementary Table 4 - siRNA sequences

Target	siRNA Sequences	Supplier
NTC (Renilla Luciferase)	Sense: CUUACGCUGAGUACUUCGA[dT][dT] Antisense: [Phos]UCGAAGUACUCAGCGUAAG[dT][dT]	Sigma-Aldrich
SAE1 (Exon 4)	Sense: GCAUGAGUUUGUAGAGGAGAA[dT][dT] Antisense: [Phos]UUCUCCUCUACAAACUCAUGC[dT][dT]	Sigma-Aldrich
SAE2 (Exon 16)	Sense: GCACCAGAUGUCCAAAUUGAA[dT][dT] Antisense: [Phos]UUCAAUUUGGACAUCUGGUGC[dT][dT]	Sigma-Aldrich

Supplementary Table 5 - Details of inhibitors

Inhibitor	Company	Catalogue Number	Target	Concentration
Colcemid	Gibco	15212012	Microtubule poison	0.05 µg/ml
Nocodazole	Sigma	1430-18-9	Microtubule poison	100 ng/ml
Panobinostat (LBH589)	SignalChem	H83-904G-SGC	Pan-HDAC inhibitor	2.5 µM
ACY-738	MedCHemExpress		HDAC 6 inhibitor	2.5 µM
RGFP966	Selleckchem	HY-19327 S7229	HDAC 3 inhibitor	2.5 µM

Supplementary Table 6 - Antibodies

Antibody (clone)	Host	Supplier	Cat. number	Lot number	Technique	Conc.	RRID
β-actin	Rabbit	Abcam	Ab8227	GR3215935-1	WB	1:3000	AB_2305186
AcK164-SAE2 (30E2-2)	Mouse	GenScript	Custom design	NA-6	WB	1:1000	N/A
SAE1	Rabbit	Abcam	ab185552	GR3379016-1	WB	1:2500	-
SAE2	Rabbit	Sigma	HRA041436	R38238	WB	1:2500	AB_2677479
Ubc9	Rabbit	Abcam	ab75854	GR118836-6	WB	1:2500	AB_1310787
SUMO1 (Y299)	Rabbit	Abcam	ab32058	GR3244068-3; GR3366977-1	WB	1:5000	AB_778173
SUMO2/3 (8A2)	Mouse	Abcam	ab81371	GR3379145-7	WB	1:5000	AB_1658424
His	Mouse	Sigma	H1029	025M4780V	WB	1:5000	AB_260015
FLAG (M2)	Mouse	Sigma Aldrich	F1804	SLBT7654	WB	1:1000	AB_262044
γH2AX	Rabbit	Abcam	Ab2893	GR3242597-1	IF	1:2000	AB_303388
αTubulin	Mouse	Santa Cruz	sc-5286	H0613	WB	1:5000	AB_628411
Vinculin [EPR8185]	Rabbit	Abcam	ab129002	GR221671-50	WB	1:2000	AB_11144129
Pericentrin	Rabbit	Abcam	ab4448	GR245491-2	IF	1:1000	AB_304461
αTubulin	Mouse	Novus	NB100-690	G-3	IF	1:1000	AB_521686
Donkey α Mouse AlexaFluor 488	Donkey	Life technologies	A21202	1975519	IF	1:5000	AB_141607
Donkey α Rabbit AlexaFluor 488	Donkey	Life technologies	A21206	1874771	IF	1:5000	AB_2535792
Donkey α Mouse AlexaFluor 555	Donkey	Life technologies	A31570	1774719	IF	1:5000	AB_2536180
Donkey α Rabbit AlexaFluor 555	Donkey	Life technologies	A31572	1945911	IF	1:5000	AB_162543
Donkey α rat AlexaFluor 555	Donkey	Life technologies	A21434	1987272	IF	1:5000	AB_2535855
Rabbit α Mouse HRP	Rabbit	Dako	P0161	20062080	WB	1:10000	AB_2687969
Swine α Rabbit HRP	Swine	Dako	P0217	20047666	WB	1:10000	AB_2728719
Mouse TrueBlot® ULTRA: Anti-Mouse Ig HRP	Mouse	Rockland	18-8817-30	39891	WB	1:5000	AB_2610849